A new simultaneous membrane thickness and catalyst loading measurement for fuel cell proton-exchange assemblies by IR transmission

We present a study of mid-infrared (mid-IR) transmission through typical proton-exchange fuel cell and water electrolyzer catalyst-coated membrane materials, and the determination of membrane layer thickness, and catalyst layer loading, from the power of the transmitted beam. Measured membrane thicknesses lay in the range of 25 to 125 μ m, and catalyst areal loadings range from 0.05 to 0.35 mg/cm². We show that the transmission spectrum correlated to membrane thickness and catalyst loading values separately, and also used a mathematical model to calculate both quantities simultaneously, from a single measurement of transmission. Measurements were carried out using a Fourier-transform infrared (FTIR) spectrometer, in specular transmission mode, in the wavelength range of 3 to 13 μ m (3333 to 770 cm⁻¹). We discuss the potential application of this method to the development of roll-to-roll manufacturing full-area-scanning quality inspection of catalyst-coated membrane (CCM) materials.

Brian G. Green, Przemyslaw Rupnowski, Scott Mauger, Michael Ulsh.

National Renewable Energy Laboratory (NREL), Golden, CO, USA.

Keywords: Proton-exchange membranes (PEM), PEM fuel cells, PEM water electrolyzers (PEMWE), catalyst-coated membranes (CCMs), quality control (QC), roll-to-roll manufacturing (R2R), Fourier-transform infrared (FTIR) spectroscopy.

Introduction

As a major component of a clean-energy future, hydrogen and fuel cell technologies provide clean, portable, high-density energy, useful in many settings including fuel cell vehicles and for operations in remote locations. Anticipating the upscaling of hydrogen technology, an appropriate large-scale manufacturing method with the potential to reduce manufacturing cost barriers is high-speed, high-volume roll-to-roll (R2R) [1,2] fabrication of membrane-electrode assemblies (MEAs), the primary electrochemical components of proton-exchange membrane (PEM) fuel cells and PEM water electrolyzers (PEMWE). Quality control (QC) methods are essential in any manufacturing system. Current MEA QC generally relies on the manual, destructive testing of MEA sample sets that are considered to be representative of entire roll goods. However, large-scale deployment of fuel cell systems will demand more stringent targets for MEA quality, reliability, and manufacturing efficiency, especially in minimizing the waste of catalytic precious metals in MEA rolls which fail inspection.

An optimal MEA QC inspection method would therefore provide non-destructive measurements, in-line with the fabrication system for real-time process control, and would allow area-scanning/full-field imaging of the full roll material. To implement measurements which are insensitive to the material vibrations realistically present in R2R systems, transmission methods have been developed including the beta- [3] and X-ray [4] gauges as point measurements for metallic and polymer films. Visible-spectrum transmission densitometry [5] is applicable to semi-transparent materials. Recent advances applying interferometric methods to electronic materials include a study [6] which compensates for material vibrations using an active feedback mechanism, achieving area scanning of photovoltaic materials in the visible spectrum, while another [7] has been used to identify defects in flexible electronics.

In the case of application to fuel cell MEA and PEMWE materials, one or more layers of carbon and/or carbon fiber are present, which are strongly absorbing and scattering in the visible spectrum, making visible interference and transmission difficult. Additionally, typical carbon layer thicknesses are on the

order of microns, which is below the detection limit [8] of some of the above methods. To meet these and other challenges and advance manufacturing QC methods for these materials, we have developed several non-destructive, in-line, area scanning techniques, including diffuse reflectance imaging [9], hyperspectral imaging [10], active thermal scanning [11], direct current (DC) electrical IR scanning [12], and reactive excitation (including reactive flow through [13,14] and reactive impinging flow [15]). These methods have demonstrated effectiveness for subsets of MEA structures: perfluorosulfonic acid (PFSA) PEMs, catalyst-coated PFSA membranes (CCMs), and diffusion media with catalyst coatings (gas-diffusion electrodes, GDEs). These in-line QC methods are capable of being integrated into R2R fabrication systems, and are area-scanning techniques which image all material passing through an inspection head.

In this work we investigated the direct, spectrally-resolved transmittance of mid-infrared (MIR) light through CCM and membrane materials, a technique amenable to future in-line, area-scanning implementation.

PFSA membranes have a polytetrafluoroethylene (PTFE) carbon-fluorine (CF) (-CF₂-)_n backbone with perfluorovinyl ether side chains, each containing a sulfonic acid (SO₃-) group. PFSA is an anionic insulator, and is a cationic conductor by means of both hopping between SO₃- groups and aqueous diffusion, and is generally chemically, thermally, and mechanically stable. Dielectric and optical properties of PFSA membranes have been studied in the ultraviolet (UV) [16], visible [17], IR [18,19,20,21], and microwave [22,23,24,25] regimes. A review of early work on IR optical properties was done by Heitner-Wirguin [26], describing study of the backbone CF₂ resonances, the degree of hydrogen bonding in hydrated PFSA, cluster phase polarities, metal binding, and the effects of different species and temperature increases on SO₃- resonances. IR reflection and absorption properties have been investigated using FTIR, infrared reflection absorption spectroscopy (IRRAS), and the insertion of luminescence probe agents. The main features of the MIR PFSA spectrum are the strong and broad

symmetric and asymmetric CF₂ absorption peaks at 9.1 μm (1100 cm⁻¹) and 8.3 μm (1200 cm⁻¹) respectively [27,28]. Areas of the absorption spectrum away from these peaks are determined by numerous, overlapping peaks associated with other species and vibrational stretching and bending modes [29] additional to those of CF₂.

Using FTIR transmittance spectroscopy, Rao [30] studies the effect of UV irradiation on the crosslinking of SO₃- groups and the presence of hydronium ions, and the consequent effects on cationic transport. From Rao's typical transmittance spectra of PFSA membranes of 180 µm thickness, we expect transmittance to vary from nearly zero at the absorption peaks to a maximum above 60% for thin samples away from the absorption peaks.

Although we find no literature on MIR transmission of catalyst layer materials (Pt or IrO₂) specifically, the dielectric [31] and optical [32,33,34] properties of solid carbon black, a typical and predominant component of catalyst materials in fuel cell electrodes and PEMWE cathodes, have been studied, as well as the optical properties of colloidal carbon black [35]. Jäger [36] describes IR absorption in carbon black as controlled by free charge carrier absorption, with steadily decreasing extinction with increasing wavelength. While far-infrared absorption depends strongly on particle morphology and agglomeration, MIR absorption depends mainly on the C-bonding character internal to particles. Absorption also depends strongly on production conditions: carbon black produced with higher pressure inert gases in the cooling phase have greater carbon sp^2/sp^3 hybridization ratios within particles, more available free carriers, and greater absorption. The same study also observes absorption peaks for hydrogen-carbon (HC) bonds when hydrogen is present as an additive. A recent study [37] on the UV/visible and IR properties of catalyst layers and inks shows that while the carbon black and ionomer volume fractions of these layers are comparable, the volume fraction of catalyst itself is small, typically less than 4%. We therefore expect both carbon black and ionomers in catalyst layers to contribute observable features to measured spectra, while catalyst features may be weak or not observed.

To estimate a minimum transmittance for a pure carbon black layer, we took the high extinction case of short wavelength of 3 μ m and high sp^2/sp^3 ratio, giving a mass extinction efficiency from Jäger [38] of $9 \cdot 10^3$ cm²/g. The transmittance T is related to the mass extinction efficiency μ_m by

$$T = I/I_0 = e^{-\mu_m \rho t},$$

where I is specular transmitted power, I_0 is incident power, ρ is mass density, and t is layer thickness. For a relatively thick catalyst coating, with a high loading of 0.4 g/cm² and typical thickness of 5 μ m, we found a MIR transmittance on the order of 10^{-2} . From this and the literature transmittance of PFSA, we expected the overall transmittance of CCM samples of varying thicknesses in both layers to be small but measurable, on the order of 10^{-3} to 10^{-1} . The mass extinction of carbon black increases steadily from the MIR to near-infrared to visible regimes, making the MIR a practical choice for spectroscopy.

The first section of this study describes the materials chosen for measurement, including fabrication conditions. This is followed by a description of characterization methods, and of parameters of the FTIR measurements. Next spectral data for the membrane and CCM materials are presented and reviewed, including noting spectral features that lend themselves to the analysis and model development of the following section. The details then follow of the expressions and parameters of the numerical model of membrane thickness and catalyst loading, and an assessment of its accuracy relative to the same characteristics measured independently. The study closes with a concluding section, and with expectations of future work.

Materials

The series of 14 samples is listed in table 1. Samples 1 through 3 were Nafion NRE211, NRE212, and N1135 PFSA membranes (Ion Power) with nominal thicknesses of 25, 50, and 89 μ m, respectively.

Sample 4 was Electro Chem EC-NM-115 PFSA membrane, with nominal thickness of 127 μ m. Liner materials were removed from membrane samples.

CCM samples were coated in-house. Samples 5-10 were fuel cell cathode single-sided CCMs with Pt catalyst with carbon support, fabricated by ultrasonic spray coating of ink onto Chemours Nafion N211 PFSA membranes, using a Sonotec ExactaCoat spray coating system. The catalyst ink included TKK TEC10E50E 50 wt% Pt powder with high surface-area carbon (HSC), with Nafion D2020, 920 EW at 20 wt%, ionomer dispersion (Ion Power), and n-propanol (nPA) and water solvent. To achieve a range of loading, the number of spray coating passes was increased over the set of samples, resulting in a range of approximately 0.05 to 0.3 mg Pt/cm². This range of loading is thought to be relevant to PEM fuel cell cathode and anode target loadings across multiple applications, as well as PEMWE cathode target loadings. The catalyst layer thickness increased correspondingly over the samples. The sprayed area was square, with 50 cm² area.

Samples 11 and 12 were PEMWE cathode single-sided CCMs with Pt catalyst and carbon support, fabricated by R2R gravure coating onto Aquivion E-98-09S PFSA membrane, with a Mini-Labo Deluxe commercial coating system (Mirwec). The catalyst ink was TKK TEC10E50E 50 wt% Pt powder with HSC, Aquivion ionomer dispersion, and nPA and water solvent. Sample 11 had a significantly less uniform coating than other samples.

Samples 13 and 14 were PEMWE anode single-sided CCMs with unsupported IrO₂ catalyst, fabricated by R2R gravure coating onto Aquivion E-98-09S PFSA membrane, with the above coating system. The catalyst ink was commercial IrO₂ powder, Aquivion ionomer dispersion, and nPA and water solvent.

Experimental methods

Table 1. Sample listing with measured PFSA thickness and Pt catalyst loading values.

Sample	Material type	PFSA thickness, µm	Catalyst loading, mg/cm ²
1	PFSA membrane	22±9.1%	0
2	PFSA membrane	51±0.98%	0
3	PFSA membrane	84±3.0%	0
4	PFSA membrane	123±1.8%	0
5	Spray-coated CCM	27±5.6%	0.062±3.3% Pt/HSC
6	Spray-coated CCM	40±4.1%	0.115±2.5% Pt/HSC
7	Spray-coated CCM	35±11%	0.162±1.8% Pt/HSC
8	Spray-coated CCM	41±4.0%	0.217±2.4% Pt/HSC
9	Spray-coated CCM	38±9,3%	0.257±1.5% Pt/HSC
10	Spray-coated CCM	43±3.5%	0.317±1.2% Pt/HSC
11	Gravure-coated CCM	90 (nominal)	0.060±82% Pt/HSC
12	Gravure-coated CCM	90 (nominal)	0.102±18% Pt/HSC
13	Grayure-coated CCM	90 (nominal)	0.396±8.0% IrO ₂
14	Gravure-coated CCM	90 (nominal)	0.357±9.7% IrO ₂

PFSA membrane thicknesses were measured using a micrometer in an uncoated region of each sample, except for samples 11-14, where no uncoated areas were present – nominal thickness is given in table 1. Three locations were measured, and the mean taken as the sample value.

CCM Pt loadings were measured using a Fischerscope XDV-SDD X-ray fluorescence (XRF) spectrometer. The source was a tungsten anode, with 50 kV voltage and 410 μ A current, and a Ni primary filter. The detector was a Si drift detector with a Be window, 30 s exposure time, and the spot diameter was 1.0 mm. Each CCM was measured at nine locations over the coated area, spaced to cover the majority of the coating. The mean was taken as the sample value. See table 1 for PFSA thickness and Pt catalyst loading results for each sample.

In this study, we analyzed MIR spectra of CCMs and membrane-only materials, taken using an FTIR spectrometer in transmission mode, and show that spectral features, described in the *Spectral analysis and model* section, correlated with PFSA thickness and catalyst loading parameters.

The spectrometer was a Thermo Nicolet 6700, with a silicon carbide (SiC) source, potassium bromide (KBr) beamsplitter, and deuterated triglycine sulfate (DTGS) detector, with a KBr window, and automatic gain. The optical velocity was 0.6329 cm/s, aperture 8 mm, spectral resolution 1.93 cm⁻¹, and four spectra were averaged together per measurement. The sample compartment was configured for measurement of specular (unscattered) transmission spectra, with samples mounted normal to the incident beam on a vertical support, and had a N₂ purge. Each sample was measured at three different locations near its center, with a separation of several mm allowed between locations. A background normalization spectrum was taken prior to each measurement. The measurement time, including background measurement, was approximately one minute.

Results

Figures 1 and 2 show the MIR direct transmittance (T) spectra for PFSA and spray-coated CCM materials, respectively, with varying thickness. Spectral signal quality provided by averaging 4 successive spectra during FTIR data collection was good over the thickness range of interest, until

approaching transmittance values less than 0.1% for the thickest samples. The T signal fell below the detection limit near the overlapping CF₂ symmetric and asymmetric absorption peaks at 8.3 and 9.1 μm [39]. Narrow absorption peaks associated with PFSA carbon-oxygen-carbon (COC), CF, and sulfur-oxygen (SO) bonds also appear in the range 9-11 μm [40]. At a wavelength value of 11.2 μm selected for later analysis (see next section), the coefficient of variance of three repeats for each sample ranged from 0.5% to 11%, with a mean over samples of 4.1%. The effect of increasing PFSA thickness or catalyst loading was large relative to the observed random error. Decreasing T with increasing membrane thickness and/or areal loading is due to the greater amount of material present in the optical path, with absorption by means of the vibrational mode and free carrier mechanisms previously mentioned for membranes and catalyst coatings, respectively.

Figure 1. MIR transmission spectra of PFSA membrane samples. Labels indicate sample numbers from table 1.

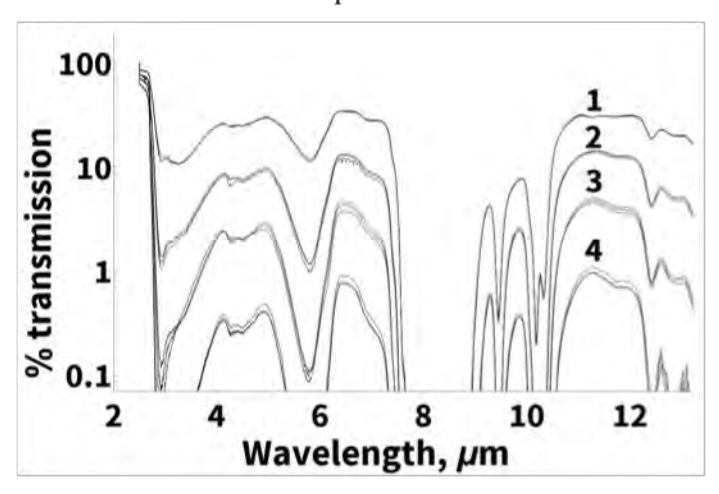
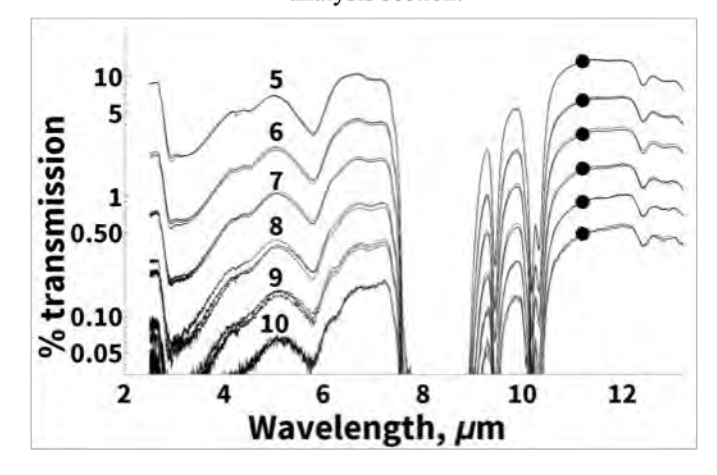


Figure 2. MIR transmission spectra of spray-coated CCM samples. Labels indicate sample numbers from table 1. The points marked at wavelength 11.2 μm are described in the spectral analysis section.



Away from the CF absorption peaks, T decreased from approximately 40% to 0.1%, depending on layer thicknesses. Due to the strong absorption in membranes at the CF absorption peaks, the T signal fell below the background noise level at these wavelengths, and the CF peaks themselves, *i.e.* T minima, could not be resolved. As the peak wavelengths are approached from below and above, broadening with increasing thickness of both PFSA and catalyst material was observed. Broadening was observed in series of films with identical compositions and coating methods, where the only nominal change was

coating thickness. The observed broadening could be homogeneous, due to shorter vibrational lifetimes in thicker films, or inhomogeneous, due to greater variation of small-scale, local stoichiometry or stresses [41] in thicker films, or a combination of homogeneous and inhomogeneous effects. In the homogeneous case, typical causes of shorter lifetimes include increased availability of thermal phonon modes in thicker films [42], and increased hydrogen bonding [43] among others.

In figure 2, we measured regular spacing in T on the logarithmic scale for CCMs with approximately equal intervals of 0.05 mg/cm² between loadings (table 1). Samples 5-10 were fabricated with the same PFSA material, with thicknesses varying less than 60%. This suggests an exponential dependence of T on loading for these CCM samples.

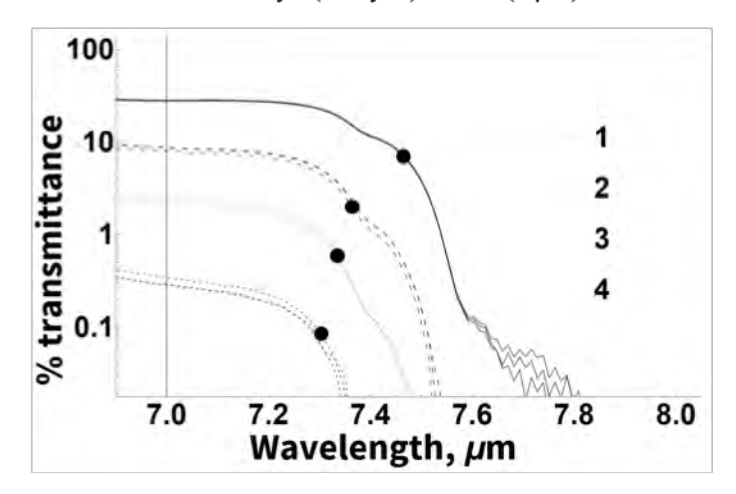
Spectral analysis and model

Definition of metrics

In order to determine the thickness of both the PFSA layer and the catalyst layer, ideally with a single measurement, a mathematical model of the two thicknesses was developed, with two independent inputs determined from the MIR T spectrum of each sample, which correlated with the two desired, independent outputs. The T value at $11.2~\mu m$ metric, referred to as 'T112', and shown as marked points in figure 2, was chosen as one such input, and depends strongly on the thickness of both the catalyst layer, and the PFSA layer.

The second metric and model input is illustrated in figure 3: its value is the wavelength in microns at which the value of T decreases to 25% of its reference value, defined as the value of T at 7 μ m, *i.e.* decay25 is defined by T(decay25) = 0.25 ·T(7 μ m). This metric was observed to depend significantly on

Figure 3. Definition of the absorption edge metric 'decay25'. Labels indicate sample numbers from table 1; samples are PFSA only. The value of T at 7 μm is used as a reference value. As thickness increases from sample 1 to 4, the wavelength where T decreases to 25% of its reference value decreases. The quantity 'decay25' is defined by T(decay25)=0.25·T(7 μm).



PFSA thickness, but only weakly on catalyst thickness, and is thus almost independent of the other metric.

Model calculation

A numerical model for PFSA thickness and catalyst loading was calculated by first fitting expressions for decay25 and T112 to measured data, giving two equations, each depending on the two variables of PFSA thickness in µm (with symbol x) and catalyst loading in mg Pt/cm² (with symbol y). The expression for decay25 was a quadratic polynomial, and for T112 was a decaying exponential, suggested by the results described in figure 2. To use the model to predict PFSA thickness and catalyst loading, the MIR T spectrum of a sample is measured, decay25 and T112 were determined from the spectrum, and those two values were taken as inputs to the numerical model. The resulting two equations in two unknowns were solved numerically to yield PFSA thickness and catalyst loading. For membrane-only materials (samples

Table 2. Numerical model parameters.

Parameter	Value $decay 25 = d_1 + d_2x + d_3x^2 + d_4y + d_5y^2$	
decay25 metric expression		
T112 metric expression	$T112 = T_1 e^{-T_2 x} e^{-T_3 y}$	
di	7.506	
\mathbf{d}_2	-0.002800	
d ₁	9.780-10-6	
d ₄	0.7043	
ds	-1.397	
T ₁	59.03	
T ₂	0.02935	
Т3	10.72	
decay25 fit R ²	0.999997	
T112 fit R2	0.997	

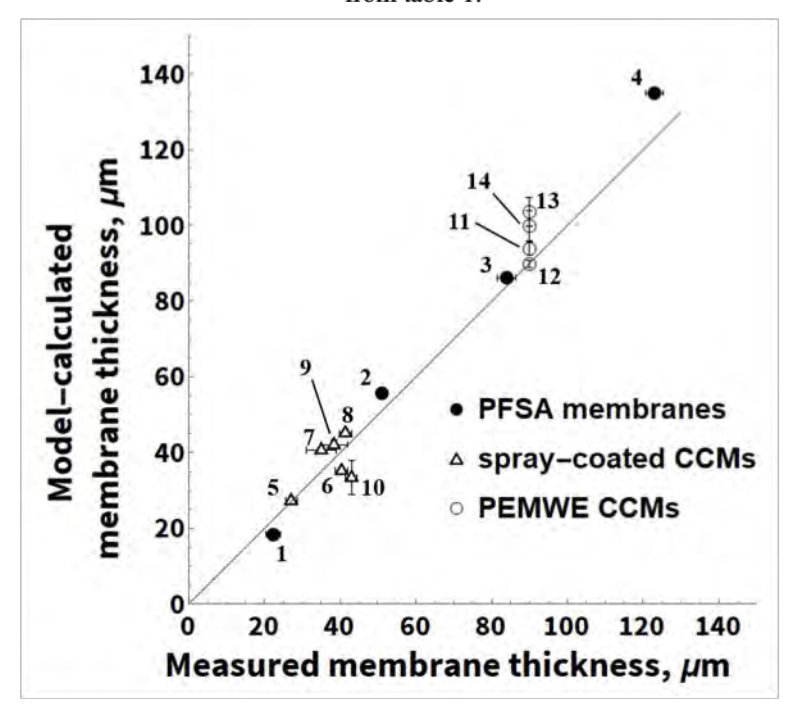
1-4), the model yielded a small negative result for loading for some samples; in these cases, the loading result was set to zero. Functional forms and parameters are given in table 2.

The reciprocals of parameters T_2 and T_3 are the 1/e penetration depth of the PFSA layer and the 1/e decay value of loading for the catalyst layer, respectively, with values 34.1 μ m and 0.093 mg Pt/cm².

Model results

Model results are compared to measured values in figures 4 and 5; vertical error bars indicate the standard deviation of three repeated measurements and model calculations, and horizontal error bars are the standard deviation of the PFSA thickness and catalyst loading measurements described in the

Figure 4. Comparison of model results for membrane thickness to measured values; the diagonal indicates exact agreement. Labels are sample numbers from table 1.



Experimental methods section. In some cases, errors are less than the width of datapoint markers. As an estimate of systematic error, for PFSA thickness, the error of the model result for individual measurements, relative to measured values, was 22% or less, and was 11% or less for 9 of the 14 samples. We note that these statements are for the sample set as a whole, including all of the PFSA membrane,

PEM CCM, and PEMWE CCM materials. For samples 11-14 (PEMWE materials), only nominal values of PFSA thickness were known.

For catalyst loading, the error was 12% or less for spray-coated PEM fuel cell CCMs (samples 5-10), but high for PEMWE materials (samples 11-14), varying between 25 to 83%. The anode samples 13 and 14 included no carbon support – a strong IR absorber – for the IrO₂ catalyst. Since the numerical model was calculated with a majority of carbon-supported catalyst layers among the samples, it is reasonable that it

would underestimate the loading for these anodes. We also expect that the discrepancies for loading for samples 11 and 12, as well as 13 and 14, could be due to differences in coating methods and composition between these and samples 1-10. In an implementation of this method in a manufacturing setting, the method is best used for materials belonging to a single set of fabrication parameters, rather than across varying parameters.

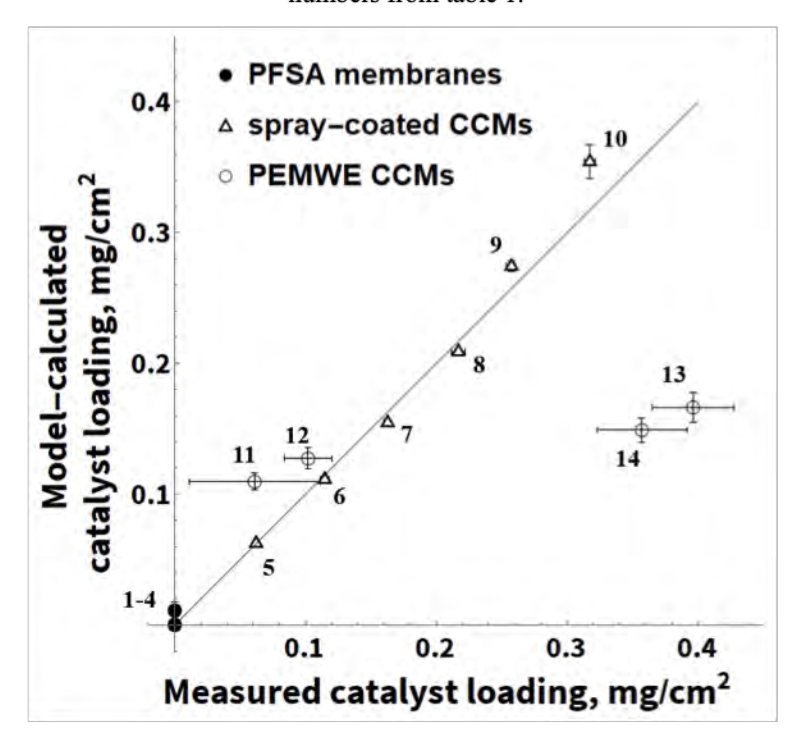
Percent differences for PFSA thickness and catalyst loading are listed by sample in table 3, calculated as the difference between the mean result over three repeats, relative to the values given in table 1. We note that several fabrication parameters were not controlled over samples, including PFSA type or brand, coating methods, ionomer content, ink ionomer to carbon weight ratio, and catalyst type or brand. It is expected that the accuracy and repeatability of this method would improve significantly with controlled fabrication parameters. Also, non-uniformity of catalyst areal density is typically in the range of 5 to 10%. It is expected that non-uniformity of PFSA thickness and catalyst loading within samples have therefore contributed significantly to discrepancies and variations. Especially for a measurement method used in a manufacturing setting, a full assessment of error would be valuable, through a gauge

repeatability and reproducibility (gauge R&R) evaluation including effects due to time, operator, and other factors.

Table 3. Accuracy of PFSA thickness and catalyst loading values calculated by the numerical model; % difference is relative to the measured values of table 1.

Sample	PFSA thickness, % difference	Catalyst loading, % difference
İ	18	~
2	9.2	-
3	2,6	~
4	9.8	-
5	0.9	0.5
6	12.8	2.8
7	16.1	4.9
8	9.2	3.5
9	9,6	6,6
10	22.4	11.7
11	4.2	82.7
12	0.9	24.8
13	15.1	58.0
14	11.0	58.3

Figure 5. Comparison of model results for catalyst loading to measured values; the diagonal indicates exact agreement. Labels are sample numbers from table 1.



Conclusions

In single-sided CCM and PFSA-only materials, PFSA thickness and the catalyst areal loading can be determined by measurement of the MIR specular transmission spectrum of the material, with a single measurement. Specific metrics in sample spectra were evaluated, and a numerical model was calculated from samples of known thickness and loading, and applied to predicting PFSA thickness and catalyst loading. This method was found to accurately predict PFSA thickness in the range 25 to 125 μ m, and catalyst loading in the range 0.05 to 0.35 mg/cm², for PFSA and PEM CCM materials, and likewise for PFSA thickness of PEMWE materials. Systematic uncertainty was significantly higher for PEMWE catalyst loading.

Systematic error in the model results for PFSA thickness and catalyst loading has been assessed by comparison to independent measurement by micrometer and XRF spectroscopy, and was found to lie below 22% for PFSA thickness. Catalyst loading systematic error was estimated to be below 12% for spray-coated PEM CCMs, but was as high as 83% for PEMWE materials. Clearly the results indicate that catalyst type (Pt/HSC vs. IrO₂) is a parameter that significantly impacts the transmittance, and it should be incorporated into the optical model once more IrO₂ specimens with various loadings are available. Moreover, we expect that model accuracy and repeatability would improve when fabrication parameters are controlled, and that a significant part of discrepancies and variation is due to material non-uniformity.

Future work

In addition to an assessment of accuracy using controlled material fabrication parameters, expected follow-on work would include extending this technique to measurement on a R2R conveyance platform. The observed accuracy of prediction, and the underlying optical properties of these hydrogen technology materials, comprise an encouraging initial step to precede any future R2R study, which would require significantly greater resources than the work presented here. An ideal, but complex, approach to R2R implementation would be developing a real-time, area-scanning FTIR transmission spectroscopy instrument for a R2R system. A more achievable approach, and likely more suited to a manufacturing setting, could rely on T measurement at specific, material-dependent wavelengths, in place of full wavelength resolution. An important consideration, from an optical perspective, for this approach would require selecting a combination of IR source, optics, and detector which would ensure sufficient throughput for a strong detected signal.

Acknowledgements

This work was authored by the National Renewable Energy Laboratory, operated by the Alliance for Sustainable Energy, LLC, for the U.S. Department of Energy (DOE) under Contract No. DE-AC36-08GO28308.

This report was funded by the Office of Energy Efficiency and Renewable Energy's (EERE) Advanced Manufacturing Office (AMO), which reorganized into the Advanced Manufacturing and Materials Technology Office (AMMTO) and the Industrial Efficiency and Decarbonization Office (IEDO) in October 2022. The views expressed in the article do not necessarily represent the views of the DOE or the U.S. Government. The U.S. Government retains, and the publisher, by accepting the article for publication, acknowledges, that the U.S. Government retains a nonexclusive, paid-up, irrevocable, worldwide license to publish or reproduce the published form of this work, or allow others to do so, for U.S. Government purposes.

References

^[1] Debe, M., Electrocatalyst approaches and challenges for automotive fuel cells, Nature 486 (2012) 43–51. https://doi.org/10.1038/nature11115

^[2] Ulsh, Michael J., Daniel, Claus, Krumdick, Gregory, Wood, David, and Prasher, Ravi, Roll-to-Roll Advanced Materials Manufacturing Lab Consortium, 2018, United States. Conference: Presented at AIMCAL R2R Conference USA 2017: Roll to Roll Web Coating and Finishing, 15-18 October 2017, Tampa, Florida. https://www.osti.gov/biblio/1482497

^[3] Ryan, D.J., Film thickness measuring method and apparatus (1975) U.S. Patent 3,860,820.

^[4] Johnson, J.T., Defect and thickness inspection system for cast thin films using machine vision and full-field transmission densitometry, Georgia Institute of Technology (2009) Ph.D. Thesis.

https://smartech.gatech.edu/bitstream/handle/1853/37234/johnson_jay_t_200912_mast.pdf?sequence=1.

^[5] Hopkinson, G.R., Goodman, T.M. and Prince, S.R., A guide to the use and calibration of detector array equipment, Spie Press, 2004.

^[6] Blunt, L., Elrawemi, M., Fleming, L., Robbins, D. and Muhamedsalih, H., In-line metrology for defect assessment on large area Roll 2 Roll substrates, 2014, Japan. Conference: Presented at 11th Laser Metrology for Precision Measurement and Inspection in Industry, 2 September 2014, Tsukuba, Japan. http://eprints.hud.ac.uk/20360/3/Nanomend_IMEKO-LMPMI_Paper.pdf.

^[7] Kimbrough, B., In-line roll-to-roll metrology for flexible electronics, Applied Advanced Optical Metrology Solutions 9576 (2015) 10-15. https://doi.org/10.1117/12.2189905.

- [8] Johnson, J.T., Defect and thickness inspection system for cast thin films using machine vision and full-field transmission densitometry, Georgia Institute of Technology (2009) Ph.D. Thesis.
- https://smartech.gatech.edu/bitstream/handle/1853/37234/johnson_jay_t_200912_mast.pdf?sequence=1.
- [9] Rupnowski, Peter, Ulsh, Michael, and Sopori, Bhushan, High Throughput and High Resolution In-Line Monitoring of PEMFC Materials by Means of Visible Light Diffuse Reflectance Imaging and Computer Vision. Conference: Presented at ASME 2015 13th International Conference on Fuel Cell Science, Engineering and Technology, American Society of Mechanical Engineers Digital Collection, 2015. https://doi.org/10.1115/FUELCELL2015-49212.
- [10] Rupnowski, P. and Ulsh, M.J., Thickness mapping using multispectral imaging (2019) U.S. Patent 10,480,935.
- [11] Rupnowski, Przemyslaw et al., In-Line Monitoring of Li-Ion Battery Electrode Porosity and Areal Loading Using Active Thermal Scanning Modeling and Initial Experiment, J. of Power Sources 375 (2018) 138–48. https://doi.org/10.1016/j.jpowsour.2017.07.084.
- [12] Aieta, Niccolo V. et al., Applying Infrared Thermography as a Quality-Control Tool for the Rapid Detection of Polymer-Electrolyte-Membrane-Fuel-Cell Catalyst-Layer-Thickness Variations, J. of Power Sources 211 (2012) 4–11. https://doi.org/10.1016/j.jpowsour.2012.02.030.
- [13] Ulsh, Michael, Porter, Jason M., Bittinat, Daniel C. and Bender, Guido, Defect detection in fuel cell gas diffusion electrodes using infrared thermography, Fuel Cells 16 (2016) 170-178. https://doi.org/10.1149/05801.0495ecst.
- [14] Das, Prodip K. et al., Rapid Detection of Defects in Fuel-Cell Electrodes Using Infrared Reactive-Flow-through Technique, J. of Power Sources 261 (2014) 401–11. https://doi.org/10.1016/j.jpowsour.2013.11.124.
- [15] Zenyuk, Iryna V. et al., Reactive Impinging-Flow Technique for Polymer-Electrolyte-Fuel-Cell Electrode-Defect Detection, J. of Power Sources 332 (2016) 372–82. https://doi.org/10.1016/j.jpowsour.2016.09.109.
- [16] De Almeida, Selma Helena and Kawano, Yoshio, Ultraviolet-Visible Spectra of Nafion Membrane, European Polym. J. 33 (1997) 1307–11. https://doi.org/10.1016/S0014-3057(96)00217-0.
- [17] Petrina, Stephanie Ann, Water Sorption, Viscoelastic, and Optical Properties of Thin NafionRTM Films, Pennsylvania State University (2013) Ph.D. Thesis. https://ui.adsabs.harvard.edu/abs/2013PhDT......223P.
- [18] Liang, Zhenxing et al., FT-IR Study of the Microstructure of Nafion® Membrane, J. of Membrane Science 233 (2004) 39–44. https://doi.org/10.1016/j.memsci.2003.12.008.
- [19] Ludvigsson, M., Lindgren, J. and Tegenfeldt J., FTIR Study of Water in Cast Nafion Films, Electrochimica Acta 45 (2000) 2267–71. https://doi.org/10.1016/S0013-4686(99)00438-7.
- [20] Rao, Arjun Sunil, et al., Role of UV Irradiation of Nafion Membranes on Ionic Groups Responsible for Proton Conduction and Mechanical Strength: A FTIR Spectroscopic Analysis, Mater. Today Communications 25 (2020) 101471. https://doi.org/10.1016/j.mtcomm.2020.101471.
- [21] Singh, Raman K., Kunimatsu, Keiji, Miyatake, Kenji, and Tsuneda, Takao, Experimental and theoretical infrared spectroscopic study on hydrated Nafion membrane, Macromolecules 49 (2016) 6621-6629. https://pubs.acs.org/doi/10.1021/acs.macromol.6b00999.
- [22] Paddison, Stephen J., Reagor, David W. and Zawodzinski Jr, Thomas A., High Frequency Dielectric Studies of Hydrated Nafion®, J. of Electroanalytical Chemistry 459 (1998) 91–97. https://doi.org/10.1016/S0022-0728(98)00321-0.
- [23] Paddison, S. J. et al., The Microwave Region of the Dielectric Spectrum of Hydrated Nafion® and Other Sulfonated Membranes, J. of New Mater. for Electrochemical Systems 3 (2000) 11.
- [24] Krishnan, Veena G. et al., The Dielectric Response of Hydrated PFSA Membranes at Microwave Frequencies Using Split Post Dielectric Resonators, ECS Meeting Abstracts 11 (2011) 542. https://doi.org/10.1149/MA2011-01/11/542.
- [25] Lu, Zijie et al., Dielectric Properties of Polymer Electrolyte Membranes Measured by Two-Port Transmission Line Technique, ECS Transactions 28 (2010) 95. https://doi.org/10.1149/1.3502448.
- [26] Heitner-Wirguin, Carla, Recent Advances in Perfluorinated Ionomer Membranes: Structure, Properties and Applications, J. of Membrane Science 120 (1996) 1–33. https://doi.org/10.1016/0376-7388(96)00155-X.
- [27] Liang, Zhenxing et al., FT-IR Study of the Microstructure of Nafion® Membrane, J. of Membrane Science 233 (2004) 39–44. https://doi.org/10.1016/j.memsci.2003.12.008.
- [28] Heitner-Wirguin, Carla, Infra-Red Spectra of Perfluorinated Cation-Exchanged Membranes, Polym. 20 (1979) 371–74. https://doi.org/10.1016/0032-3861(79)90103-4.

- [29] Singh, Raman K., Kunimatsu, Keiji, Miyatake, Kenji, and Tsuneda, Takao, Experimental and theoretical infrared spectroscopic study on hydrated Nafion membrane, Macromolecules 49 (2016) 6621-6629. https://pubs.acs.org/doi/10.1021/acs.macromol.6b00999.
- [30] Rao, Arjun Sunil, et al., Role of UV Irradiation of Nafion Membranes on Ionic Groups Responsible for Proton Conduction and Mechanical Strength: A FTIR Spectroscopic Analysis, Mater. Today Communications 25 (2020) 101471. https://doi.org/10.1016/j.mtcomm.2020.101471.
- [31] Moalleminejad, Morteza and Chung, D. D. L., Dielectric Constant and Electrical Conductivity of Carbon Black as an Electrically Conductive Additive in a Manganese-Dioxide Electrochemical Electrode, and Their Dependence on Electrolyte Permeation, Carbon 91 (2015) 76–87. https://doi.org/10.1016/j.carbon.2015.04.047.
- [32] O'Reilly, J. M. and Mosher, R. A., Functional Groups in Carbon Black by FTIR Spectroscopy, Carbon 21 (1983) 47–51. https://doi.org/10.1016/0008-6223(83)90155-0.
- [33] Jäger, C. et al., Spectral Properties of Carbon Black, J. of Non-Crystalline Solids 258 (1999) 161–79. https://doi.org/10.1016/S0022-3093(99)00436-6.
- [34] Alcántara, Ricardo et al., Carbon Black: A Promising Electrode Material for Sodium-Ion Batteries, Electrochemistry Communications 3, (2001) 639–42. https://doi.org/10.1016/S1388-2481(01)00244-2.
- [35] Janzen, Jay, The Refractive Index of Colloidal Carbon, J. of Colloid and Interface Science 69 (1979) 436–47. https://doi.org/10.1016/0021-9797(79)90133-4.
- [36] Jäger, C. et al., Spectral Properties of Carbon Black, J. of Non-Crystalline Solids 258 (1999) 161–79. https://doi.org/10.1016/S0022-3093(99)00436-6.
- [37] Jacobsen D., Porter J., Ulsh M., Rupnowski P., Spectroscopic Investigation of Catalyst Inks and Thin Films Toward the Development of Ionomer Quality Control, Appl. Spectroscopy 76 (2022) 644-659. https://doi.org/10.1177/00037028221080177.
- [38] Jäger, C. et al., Spectral Properties of Carbon Black, J. of Non-Crystalline Solids 258 (1999) 161–79. https://doi.org/10.1016/S0022-3093(99)00436-6.
- [39] Liang, Zhenxing et al., FT-IR Study of the Microstructure of Nafion® Membrane, J. of Membrane Science 233 (2004) 39–44. https://doi.org/10.1016/j.memsci.2003.12.008.
- [40] Liang, Zhenxing et al., FT-IR Study of the Microstructure of Nafion® Membrane, J. of Membrane Science 233 (2004) 39–44. https://doi.org/10.1016/j.memsci.2003.12.008.
- [41] Gunde, M.K., Vibrational modes in amorphous silicon dioxide. Physica B 29 (2000) 286-295. https://doi.org/10.1016/S0921-4526(00)00475-0.
- [42] Colthup, N., Introduction to infrared and Raman spectroscopy, second ed., Academic Press, New York, 1975.
- [43] Athokpam, B., Ramesh, S.G. and McKenzie, R.H., Effect of hydrogen bonding on the infrared absorption intensity of OH stretch vibrations, Chemical Physics 488 (2017) 43-54. https://doi.org/10.1016/j.chemphys.2017.03.006.